Master's Thesis

The role of cellular cytoskeleton in the egress of Coxsackievirus B3

Juho Niva

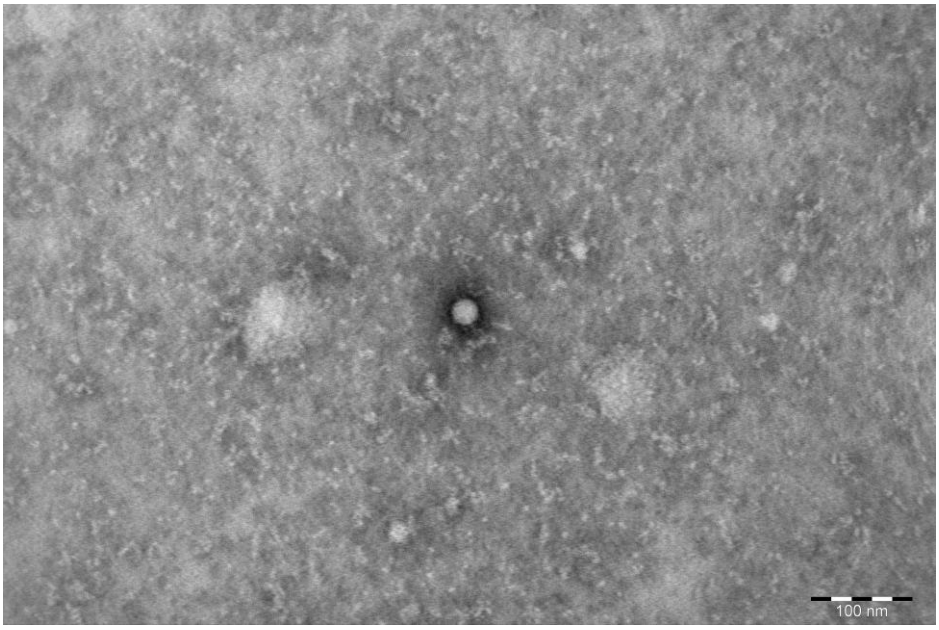

Electron microscope (EM) image of negative stained Coxsackievirus B3 capsid.

University of Jyväskylä

Department of Biological and Environmental Science

Cell and molecular biology

25 October 2020

UNIVERSITY OF JYVÄSKYLÄ, Faculty of Mathematics and Science
Department of Biological and Environmental Science
Cell and molecular biology

Juho Niva: The role of cellular cytoskeleton in the egress of Coxsackievirus B3
MSc thesis: 37 p.
Supervisors: Docent Maija Vihinen-Ranta and MSc Outi Paloheimo
Reviewers: PhD Vesa Aho and Prof. Varpu Marjomäki
October 2020

Keywords: coxsackievirus B3, cell cytoskeleton, egress

Coxsackievirus B3 (CVB3) is an enterovirus that has an impact on severe diseases including myocarditis, cardiomyopathy, and type 1 diabetes. The infection of CVB3 has been noticed to alter the morphology of green monkey kidney cells by forming cage-like protrusions to the host cell membrane. The protrusions were found packed with actin filaments and viral capsids, thus, hypothesizing an atypical, non-lytic way of spreading from the host cell to another. To further examine the non-lytic pathway and the role of cellular cytoskeleton, stabilizing and depolymerizing inhibitors of actin and microtubules were used. The inhibition of myosin II, myosin light chain kinase (MLCK), RhoA-kinase (ROCK) and mitogen-activated kinase were also examined to see the structural and transcriptional effect on the morphological changes and protrusion formation. The CVB3-infected and drug-treated GMK cells were analyzed with fluorescent-activated cell sorting (FACS) and confocal laser scanning microscopy. Our analyses showed that inhibition of the cytoskeleton filaments and cell kinases decreases the number of CVB3 infected cells. According to the confocal microscopy images, the strongest inhibitors (phalloidin and nocodazole) also prevented some of the characteristic changes in the cell morphology normally seen in CVB3 infection. Our findings also suggest that inhibition of ROCK or MLCK or actin stabilizing with phalloidin could interfere with the nonlytic egress of CVB3. Although, microtubule depolymerization significantly inhibited the number of CVB3 infected cells, the microtubule inhibition did not prevent the emergence of CVB3-induced protrusions. Overall, our results were promising, and this work further establishes that a dynamic actin cytoskeleton plays an essential role in the possible non-lytic egress of CVB3.

JYVÄSKYLÄN YLIOPISTO, Matemaattis-luonnontieteellinen tiedekunta
Bio- ja ympäristötieteiden laitos
Solu- ja molekyylibiologia

Juho Niva: Solutukirangan rooli Coxsackievirus B3:n poistumiseeen
Pro gradu -tutkielma: 37 s.
Työn ohjaajat: Dosentti Maija Vihinen-Ranta ja FM Outi Paloheimo
Tarkastajat: FT Vesa Aho ja Prof. Varpu Marjomäki
Lokakuu 2020

Hakusanat: coxsackievirus B3, solutukiranka, poistuminen

Enterovirus-sukuun kuuluva Coxsackievirus B3 aiheuttaa vakavia sairauksia mm. sydänlihastulehdusta, kardiomyopatiaa ja tyypin 1 diabetesta. CVB3 on yksijuosteita RNA:ta sisältävä virus, joka replikoituu solun sytoplasmassa. CVB3 infektion loppuvaiheessa solun solukalvosta kuroutuu ulospäin aktiinia sisältäviä pitkänomaisia kalvoulkonemia. Näiden rakenteiden on arveltu mahdollistavan CVB3-virukselle epätyypillisen, ei-lyyttisen poistumisen isäntäsolusta ja leviämisen solusta toiseen. Tässä työssä tarkasteltiin viruksen solusta poistumista ja selvitettiin miten solutukirankaan vaikuttavat inhibiittorit säätelevät CVB3-infektion etenemistä ja viruksen aiheuttamien kalvoulkonemien muodostumista green monkey kidney (GMK) soluissa. Käytimme inhibiittoreita, jotka aiheuttavat aktiinitukirangan ja mikrotubulusten stabiloimisen tai depolymerisaation. Lisäksi tutkimme miten myosiini II:n, myosin light chain -kinaasin (MLCK), RhoA-kinaasin (ROCK) ja MAP-kinaasin inhibitio vaikuttaa viruksen aiheuttamiin morfologisiin muutoksiin ja kalvoulkonemien muodostumiseen. Analysoimme CVB3-infektoituja ja inhibiittorikäsiteltyjä apinan munuaissoluja virtaussytometriaa ja konfokaalimikroskopiaa hyödyntäen. Analyysiemme tulokset osoittivat, että solutukirangan molekyyleja ja kinaaseja inhiboimalla, infektoituneiden GMK solujen määrä pieneni merkittävästi. Mikroskooppikuvista nähdään, että jotkut inhibiittorit (phalloidin ja nocodazole) myös ehkäisivät CVB3-infektion aiheuttamia morfologisia muutoksia GMK soluissa. Lisäksi huomasimme, että ROCK:n ja MLCK:n inhibointi tai aktiinitukirangan stabiloiminen phalloidiinilla, mahdollisesti heikentää CVB3-partikkeleiden ei-lyyttistä poistumista isäntäsolusta. Vaikka mikrotubulusten kemiallinen pirstominen vähensi huomattavasti CVB3-infektoitujen solujen määrää, ei mikrotubulusten inhibitio kuitenkaan estänyt CVB3:n aiheuttamien kalvoulkonemien syntymistä Tutkimustuloksemme tukee dynaamisen aktiinitukirangan merkitystä CVB3:n ei-lyyttiselle poistumiselle.

TABLE OF CONTENTS

ABBREVIATIONS

CAR	Coxsackie and adenovirus receptor
CVB	Coxsackievirus group B
CytD	Cytochalasin D
DAF	Decay-acceleration factor
DMEM	Dulbecco's Modified Eagle Medium
FACS	Fluorescent-activated cell sorting
FC	Flow cytometry
GMK cells	Green monkey kidney cells
HFMD	Hand, foot and mouth disease
JAS	Jasplakinolide
LatA	Latrunculin A
MLCK	Myosin light chain kinase
MOI	Multiplicity of infection
MT	Microtubules
NM-II	Nonmuscle myosin II
NOC	Nocodazole
PAC	Paclitaxel
ROCK	Rho-associated kinase

1. INTRODUCTION

1.1. Coxsackieviruses

Coxsackieviruses (CV) are a group of positive-sense single-stranded RNA (+ssRNA) viruses that usually causes intestinal infections in humans. Coxsackieviruses belong to the family *Picornaviridae* and genus *Enterovirus* that also includes polioviruses and enteroviruses. CVs are divided into two groups (A and B) according to the symptoms which were seen in mice in the early observations. Group A has 24 serotypes CVA1-24 and group B has 8 serotypes CVB1-8. In humans, both coxsackie group viruses normally cause mild symptoms that include fever and stomach pain. Patients are typically cured after 10 - 12 days post-infection. The infection usually occurs orally and the virus replicates in the intestines. Group A viruses can cause hand, foot and mouth disease (HFMD) in young infants. When escaping the intestinal tract coxsackieviruses can cause much more severe illnesses such as viral myocarditis and pancreatitis (Tracy et al., 2000).

1.2 CVB3 structure and life cycle

Like most viruses, coxsackievirus B3 (CVB3) is host-dependent, needing a host cell for replication. Coxsackievirus B3 has a single-stranded, positive-sense RNA genome of 7,400-nucleotides that encodes 11 different proteins. It has an icosahedral viral capsid (~30nm) with three external protein subunits VP1, VP2, V3 and one internal subunit VP4. CVB3 is a non-enveloped, “naked”, virus and does not have a lipid membrane around the capsid. CVB3 is known to bind two cell membrane receptors: coxsackie and adenovirus receptor (CAR), which is located in the tight junctions, and decay-acceleration factor (DAF). The different CVB3 strains differ in their abilities to bind either CAR only or both DAF/CAR receptors. It has been suggested that CAR is essential for viral entry, whereas DAF forms clusters with CVB3, essentially helping the virus to reach the tight junctions (Coyne and Bergelson, 2006). CAR is important for the release of the viral RNA genome from the capsid after endocytosis (Milstone et al., 2005). After binding to the host cell membrane receptor, the virus is taken inside the host cell by endocytosis. It has been suggested by Chung et al. (2005) who showed that CVB3 uses clathrin-mediated endocytosis as an entry pathway (Chung et al., 2005). Inside the cell the capsid is uncoated, and the RNA genome is released into the cytoplasm following the translation of one large polyprotein. This polyprotein is cleaved into structural proteins (VP’s) and

non-structural proteins. The viral genome is transcribed and eventually, new virions are assembled. New procapsids are self-assembled from viral RNA and 60 copies of structural proteins VP1, VP3 and VP0. Later the VP0 self-cleaves into mature VP2 and VP4 subunits and the final assembly of the capsid occurs (Stanway and Hyypiä, 1999). The replication process of CVB3 occurs in the outer surface of virus-induced autophagosomes (Wong et al., 2008). Finally, the mature CVB3 virions trigger the host cell apoptosis via caspase activation, followed by cell lysis and the release of viral particles out of the cell. Though CVB3 is assumed to exit the host cell via cell lysis, an alternative pathway has been suggested (Paloheimo et al., 2011). In their study, Paloheimo et al. (2011) introduced CVB3-induced cellular protrusions in green monkey kidney (GMK) cells and suggested that the protrusions could be used by the CVB3 for the non-lytic egress from a host cell to another. The non-lytic exit of non-enveloped viruses has been previously demonstrated, for example, with poliovirus, rice gall dwarf virus, and hepatitis A virus (Bird and Kirkegaard, 2015; Wei et al., 2006; Feng et al., 2013). The non-lytic pathway is thought to be crucial for persistent enterovirus infections. The CVB3-induced protrusions, as shown by Paloheimo et al., form cage-like structures to adjacent cells and are rich in viral capsid, actin and microtubules. Furthermore, the CVB3 was also able to infect other adjacent cells in the presence of a neutralizing antibody. These findings indicate that the virus could spread directly from a host cell to another. Paloheimo et al. (2011) also showed that microtubule depolymerization did not inhibit viral capsid localization to protrusions, but that actin disintegration resulted in cytoplasmic accumulation of viral particles (Paloheimo et al., 2011). Hence, the critical role of the actin cytoskeleton in viral capsid movement along the protrusions was proposed.

1.3 Cell cytoskeleton

The cell cytoskeleton consists of three major filaments: intermediate filaments (IF), microtubules (MT) and actin filaments. All filaments are built from small protein subunits that are attached to each other via hydrophobic interactions and weak non-covalent bonds. This allows for these subunits to diffuse quickly inside the cell, providing rapid structural reorganization of the filaments when needed. Intermediate filaments are only found in eukaryotic cells that are exposed to mechanical stress. Intermediate filament subunits are longer and elastic while microtubule and actin subunits are globular and compact.

Microtubules are composed of heterodimer tubulin subunits which consist of two closely related α-tubulin & β-tubulin molecules tightly bound together. Both α- & β-tubulin bind GTP nucleotides but the GTP hydrolysis only occurs in β-tubulin which has an important role in the dynamics of microtubule filaments. Each microtubule has 13 parallel protofilaments attached to each other forming a hollow cylindrical tube (Figure 1.). The addition and loss of tubulins occur almost always in the ends of microtubule filaments. The β-tubulins are exposed to the plus end and α-tubulins are in the minus end of microtubules. Thus, microtubules have a structural polarity, and the growth of the filament is faster at the plus end.

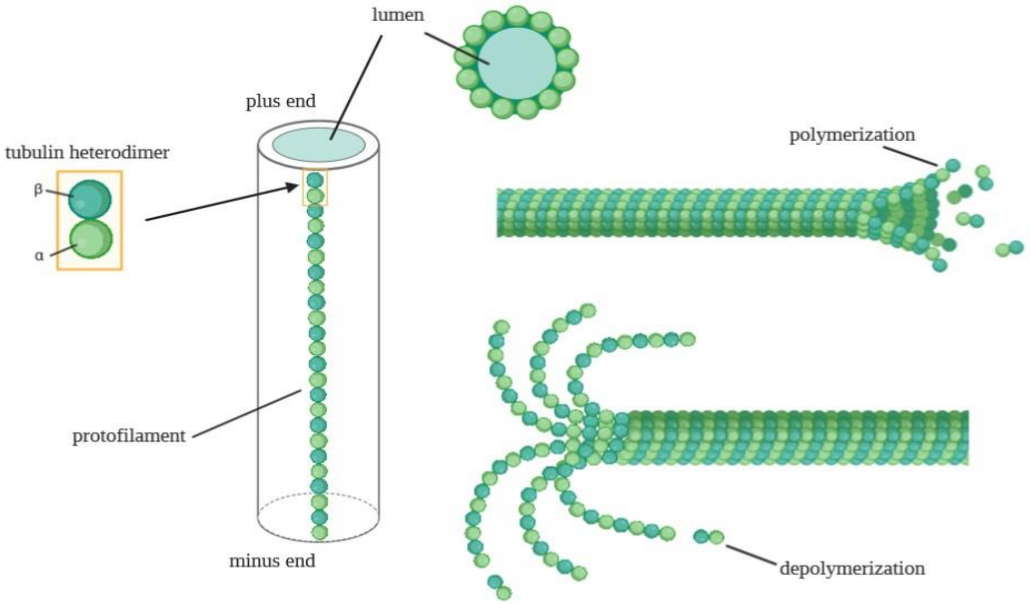

Figure 1. The structure of microtubules. The tubulin heterodimer has two different tubulin molecules α-tubulin & β-tubulin. Tubulins create a rod-shaped structure called protofilament and 13 protofilaments then initially build the hollow and cylindrical tube, the microtubule. Microtubules are unstable and they undergo constant polymerization and depolymerization. Picture made with Biorender (www.biorender.com).

Like microtubules, actin filaments are also built from globular adjacent protein subunits (G-actin) attached to each other forming filamentous structures. The actin molecule is a monomer and instead of GTP, it binds to ATP (or ADP) nucleotide. Actin filament (F-actin) has a helical structure and like microtubules, it has a structural polarity that is caused by the ATP and ADP binding site (Figure 2.). Historically the minus end is also called the "pointed end" and the plus end as the "barbed end".

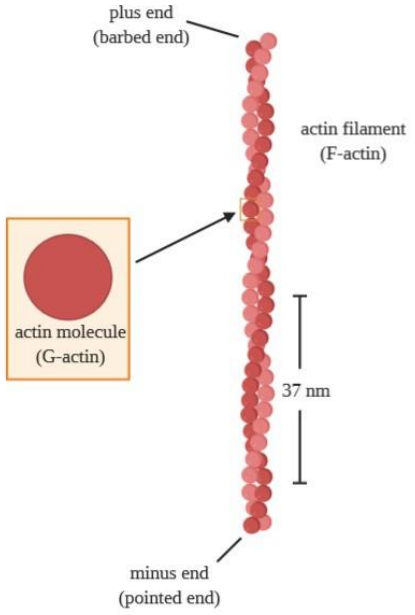

Figure 2. The structure of the actin filament. The actin molecule (G-actin) is a polypeptide that binds to an ATP or ADP nucleotide and has polarity caused by the nucleotide-binding notch at the minus end. Each actin filament (F-actin) is built from several adjacent actin molecules. The filament has a helical structure, due to two protofilaments that twist around each other in a 37nm long right-handed helix. Picture made with Biorender.

Both microtubules and actin filaments play a major role in several viral infections (Bearer and Satpute-Krishnan, 2002; Gil et al., 2017; Walsh and Naghavi, 2019). The actin cytoskeleton of the host cell is used by many viruses in all stages of the infection, from entry through replication to egress. Viruses like murine leukemia virus (MLV), human immunodeficiency virus (HIV-1), papillomaviruses (PV), and vaccinia virus (VV) move along the host cell outer membrane towards the entry site (Lehmann et al., 2005; Cudmore et al., 1995; Schelhaas et al., 2008). This "virion surfing" happens as a result of the virus binding to specific receptors that trigger myosin motors to contract cortical actin under the cell membrane (Lehmann et al., 2005; Smith et al., 2008). HIV-1 binding also triggers membrane receptor clustering of CD4 and CXC-cytokine receptor 4, yet another actin-mediated process important for successful viral entry (Vorster et al., 2011; Iyengar et al., 1998). In the clathrin-mediated entry of CVB3 and adenoviruses, cortical actin in the cell membrane is activated by binding to the DAF receptor. This binding leads to the reorganization of actin and allows the virus to reach the necessary CAR receptor hidden in the tight junctions (Coyne and Bergelson, 2006). It has been previously shown that disruption of F-actin leads to the inhibition of HIV-1 entry but also to reverse

transcription, reduced virion assembly and budding (Bukrinskaya et al., 1998). The CVB3-induced protrusions in the GMK cells were found rich in actin and viral capsid proteins, and similar looking actin-rich structures have been found from HIV-1 infected macrophages (Rustom et al., 2004; Hashimoto et al., 2016). These structures, known as tunneling nanotubes (TNT), extend from the host cell to another and can be up to 100nm long. TNT's transport several cellular molecules, proteins, and organelles, like mitochondria. It has also been suggested that the HIV-1 virus could use TNT's to move between host cells, avoiding viral antibodies and other antiviral components (Hashimoto et al., 2016).

1.3 Motor proteins

Like cell cytoskeleton molecules, motor proteins are involved in cell motility but also in the transport of cellular molecules, by moving along cytoskeleton filaments. Microtubules have two major motor protein families: kinesin and dynein, whereas actin only pairs with nonmuscle myosin II (NM-II). Many viruses use the cellular motor proteins for moving viral proteins, genome, or capsids inside the cell. Herpes simplex virus 1 (HSV-1) has been found to use both MT and actin in virus transport (Lyman and Enquist, 2009). It is proposed that HSV-1 uses MT for long-range movement along the axons and actin-myosin for short-range movement in the cell and nerve ends. The actin-myosin network has many functions in cell motility and intracellular organization (Munjal and Lecuit, 2014). Nonmuscle myosin is activated by several kinases, such as RhoA-kinase (ROCK) and myosin light chain kinase (MLCK), through the phosphorylation of the myosin light chain (MLC) (Tan and Leung, 2009; Totsukawa et al., 2000; Amano etal., 2010). Indeed, cell-cell transmission of HIV-1 is blocked when either LIM-kinase (LIMK1) or ROCK1 was inhibited (Wen et al., 2014). Additionally, the inhibition of MLCK and NM-II disturb HSV-1 entry and spreading to neighboring cells (Antoine and Shukla, 2014).

2. AIMS OF THE STUDY

CVB3 viral particles normally exit the host cell via cell lysis by disrupting the cell membrane. However, previous studies have demonstrated that CVB3 infection alters the host cell morphology, and that actin-containing plasma membrane protrusions emerge at the late stage of the infection (Paloheimo et al., 2011). These studies suggested that these cellular protrusions are involved in cellular egress and transmission of progeny capsids to the neighboring cells. Although, the cellular egress is potentially dependent on virus-induced protrusions, it is currently undefined what the specific role of the cytoskeleton is when progeny virus capsids exit the host cell through these cellular protrusions. To study further this issue two hypotheses were set for the study.

I Inhibitors affecting the action of cellular cytoskeleton hinder capsid egress.
II The actin cytoskeleton and its motor proteins have a role in capsid egress.

3. MATERIAL AND METHODS

3.1 Viruses and cells

Nancy strain of CVB3 virus was acquired from American Type Culture Collection (ATCC, Manassas, VA). Green monkey kidney (GMK) cells were cultured at 37°C 5% CO_2 in Earle's minimum essential medium (MEM) with added 1% glucose, 10% heat-inactivated fetal calf serum (FCS), 0,05mg/ml penicillin, 0,05mg/ml streptomycin (PAA laboratories, GmbH, Linz, Austria) antibiotics, 1mM L-glutamine (Invitrogen, Carlsbad, CA). The infection was done by adding CVB3 to the cell culture and kept at 37°C until fixation was performed.

3.2. Antibodies and chemicals

Flow cytometry of cell-associated viral proteins was done with an anti-CVB3 monoclonal antibody (Millipore, Billerica, MA) conjugated to Atto488-fluorophore according to the manufacture's protocol (Innova Biosciences, Cambridge, UK). Immunostaining for confocal microscopy of CVB3 viral capsid proteins was done with CVB3 polyclonal antibody (Ab) (Pharmacia Fine Chemicals, Uppsala, Sweden) followed by staining with Alexa Fluor 488-conjugated anti-rabbit IgG secondary antibody (Molecular Probes). Microtubules were labeled with α-tubulin mAb (Amersham, Buckinghamshire, UK) and Alexa Fluor 633 or 488 conjugated anti-Mouse IgG secondary antibody (Molecular Probes). Actin filaments were visualized with FITC-Phalloidin (Molecular Probes). A total of 11 different inhibitors of actin filaments, microtubules, myosin light chain kinase, MAPK kinase and RhoA kinase were used in the experiments (Table 3.1). The inhibitors were chosen by their ability to directly or indirectly alter the cytoskeleton molecules that CVB3 viral particles assumingly could use in the egress from the infected cells. The final concentration of each inhibitor was searched from literature and optimized prior to the experiments.

Table 3.1. List of inhibitors used in the experiments.

Inhibitor	Target and mechanism	Product (Cat#)	Final concentration
Latrunculin A	actin depolymerization	*Sigma-Aldrich, #L5163*	5µM
Jasplakinolide	actin depolymerization	*Sigma-Aldrich, #J4580*	2µM
Cytochalasin D	actin filament stabilization	*Sigma-Aldrich, #C8273*	20µM
Phalloidin	actin filament stabilization	*Sigma-Aldrich, #P2141*	25µM
Paclitaxel	microtubule stabilization	*Sigma-Aldrich, #T7191*	2µM
Nocodazole	microtubule depolymerization	*Sigma-Aldrich, #M1404*	50µM
Blebbistatin	myosin II ATPase	*Sigma-Aldrich, #B0560*	50µM
ML-7	myosin light chain kinase (MLCK)	*Sigma-Aldrich, #I2764*	50µM
U0126	mitogen-activated protein kinase (ERK 1/2)	*Cell Signaling Technology, #9903*	20µM
AMTZD	mitogen-activated protein kinase (ERK 1/2)	*Sigma-Aldrich, #A6355*	50µM
Y-27632	RhoA kinase (ROCK)	*Sigma-Aldrich, #Y0503*	50µM

3.3 Flow cytometry

The effect of inhibitors on the CVB3 infection was analyzed with fluorescent-associated cell sorting (FACS). Virus proteins were detected with Atto488-conjugated CVB3 mAb (1 µg/1 x 10^6cells). The GMK cells were cultured in 75 cm^2 flasks and subcultured two days prior to the FACS experiment. Subculturing was done from a confluent flask by adding 200 µl of cell suspension (diluted 1:10 in MEM) to the 8,8 cm^2 plate with 2 ml of medium. The cells were left to attach and proliferate for 32 - 48 hours. The infection with CVB3 (MOI 0.2) was performed 24 hours before the FACS analysis and the inhibitors were added 12 hours post-infection (hpi). After 24 hpi the cells were detached by scraping, transferred to 2 ml microcentrifuge tubes, and centrifuged for 5 min at 16 000 RCF (13 000 ×g). The suspension medium was removed, and the cell pellet was washed with phosphate-buffered saline (PBS) and centrifuged for 5 min at 16 000 ×g. The cells were then fixed by re-suspending them

in 500 µl of Flow Cytometry Fixation buffer (#FC004, R&D Systems Inc.). The cells were incubated at room temperature for 15 minutes and mixed every 5 minutes. 500 µl of 1X PBS was then added and the samples were centrifuged for 5 min at 16 000 ×g. The fixation solution was removed, and the samples were washed with 1X PBS by centrifuging for 5 min at 16 000 ×g. The PBS was then removed, and the cells re-suspended in 100 µl of Flow Cytometry Permeabilization/Wash Buffer (#FC005, R&D Systems Inc.). Atto488-conjugated CVB3-MAb (Millipore, Billerica, MA) was added and the samples were incubated for 1-2 hours at +4 °C. After incubation, 400 µl of Flow Cytometry Permeabilization/Wash Buffer (1X) was added and the samples centrifuged for 5 min at 16 000 RCF. The cell pellet was resuspended in 400 µl of Flow Cytometry Staining Buffer (R&D Systems, Catalog # FC 001) and the sample tubes were kept on ice until the next stage of the experiment. Before measuring, each sample was pipetted through a filter paper into a 10 mL glass tube. A total of 4×10^4 cells was calculated per measurement and repeated 3 to 4 times for both experiments. FACS experiments were performed with FACSCalibur and CellQuest software (Becton Dickinson, Heidelberg, Germany).

3.4. Confocal microscopy

Laser scanning confocal microscopy imaging was used to visualize both the CVB3 and inhibitor induced morphological changes in GMK cells. The cells were cultured for two days in 8,8 cm^2 plates with coverslips. The infection was added by pipetting 20 µl of CVB3 solution (MOI: 0.2) to the plate. The inhibitors were added to the plate 12 hours after CVB3 infection and the cells were fixed after 24 hpi with 4% paraformaldehyde (PFA) for 20 – 60 minutes at room temperature (RT). The fixed cells were immunolabeled indirectly with fluorescent markers. Primary labeling was done by incubating the cells for 60 min at RT with primary antibodies diluted in permeabilization buffer. After primary antibody labeling, the unbound antibodies were removed by washing the cells with 1X PBS. The secondary fluorescent-conjugated antibodies were attached by incubating them for 30 minutes at RT. The unbound antibodies were removed by washing with 1X PBS. The coverslips were then mounted to the microscope slides with Mowiol-Dabco (25mg/ml) and kept in the dark at +4 °C until imaging. The imaging was completed with Olympus Fluoview 1000 (FV-1000) confocal microscopy. Alexa Fluor 488-conjugated antibodies were excited with a 488 nm argon laser, Alexa Fluor 555 with 543

nm He-Ne laser and Alexa Fluor 633 with 633 nm He-NE laser. Fluorescence was collected with a 510 to 540 nm band-pass filter (AF488), 570 to 6200nm band-pass filter (AF555) and 647 nm long-pass filter (AF633). The image analysis was performed with Fiji image analysis software.

4. RESULTS

4.1 Flow cytometry

Flow cytometry experiments were carried out to examine the effect of the cytoskeleton molecule and motor protein inhibitors to CVB3 infection success. The main interest was to see how inhibitors affect the spreading of CVB3 viral particles after the infection has been active for 12 hours.

Table 4.1. The effect of inhibitors to the CVB3 infection. Two separate experiments (E1 and E2) were carried out and the number of CVB3-mAb labeled cells (%) was counted from a total number of 4 x 10^4 cells. Each sample plate was measured 3 to 4 times and the mean number of CVB3-infected cells (%) was calculated. The data shows the mean number of CVB3-mAb labeled cells (%) on each sample plate of two experiments (E1 and E2). Finally, the average number of CVB3-mAb labeled cell (%) was calculated from the two experiments (E1+E2) to estimate the effect of each inhibitor. Mean standard deviation (SD) between the two experiments was also calculated for each sample.

Sample	E1 (% CVB3-Mab)	E2 (% CVB3-Mab)	E1+E2 (% CVB3-Mab)	SD
Uninfected (C-)	5,64	5,24	5,44	0,20
CVB3 only (C)	60,91	70,18	65,55	4,63
Latrunculin A (5µM)	66,98	53,85	60,42	6,56
Jasplakinolide (2µM)	52,42	53,75	53,09	0,65
Cytochalasin D (20µM)	52,41	46,22	49,32	3,10
Phalloidin (25µM)	43,91	35,47	39,69	4,22
Paclitaxel (2µM)	51,14	68,48	59,81	8,67
Nocodazole (50µM)	40,53	41,71	41,12	0,59
Blebbistatin (50µM)	76,25	67,12	71,69	4,57
ML-7 (50µM)	30,62	33,82	32,22	1,60
U0126 (20µM)	58,1	74,38	66,24	8,14
AMTZD (50µM)	54,33	53,08	53,71	0,62
Y-27632 (50µM)	50,3	56,9	53,60	3,30

The inhibiting drugs were added 12 hpi. and the cells were fixed at 24 hpi. The number of CVB3-mAb labeled cells were counted from a total of 4 x 10^4 cells and measurement was repeated 3 to 4

times for each sample. The results of the flow cytometry experiments are shown in Table 4.1. The specificity of the CVB3 antibody in flow cytometry was evaluated by adding the Atto488-conjugated CVB3-mAb to the uninfected cells (C-). The level of unspecific binding was similar in both experiments 5,64% (E1) and 5,24% (E2). The number of CVB3-infected cells 24 hpi was 60,91% (E1) and 70,18% (E2) and the average number of CVB3-infected cells (E1+E2) in the positive control (C) was 65,55 % ± 4,32 (SD). Overall, most of the inhibitors decreased the number of CVB3 infected cells. In the second experiment, both Latrunculin A and Blebbistatin showed an increased number of CVB3-Mab labeled cells. The same effect was seen in the first experiment with the U0126. However, prior to the experiments, during optimization (data not shown), all of the drugs inhibited the CVB3 infection. The increased number of CVB3-infected cells during the experiments is most likely due to a technical error.

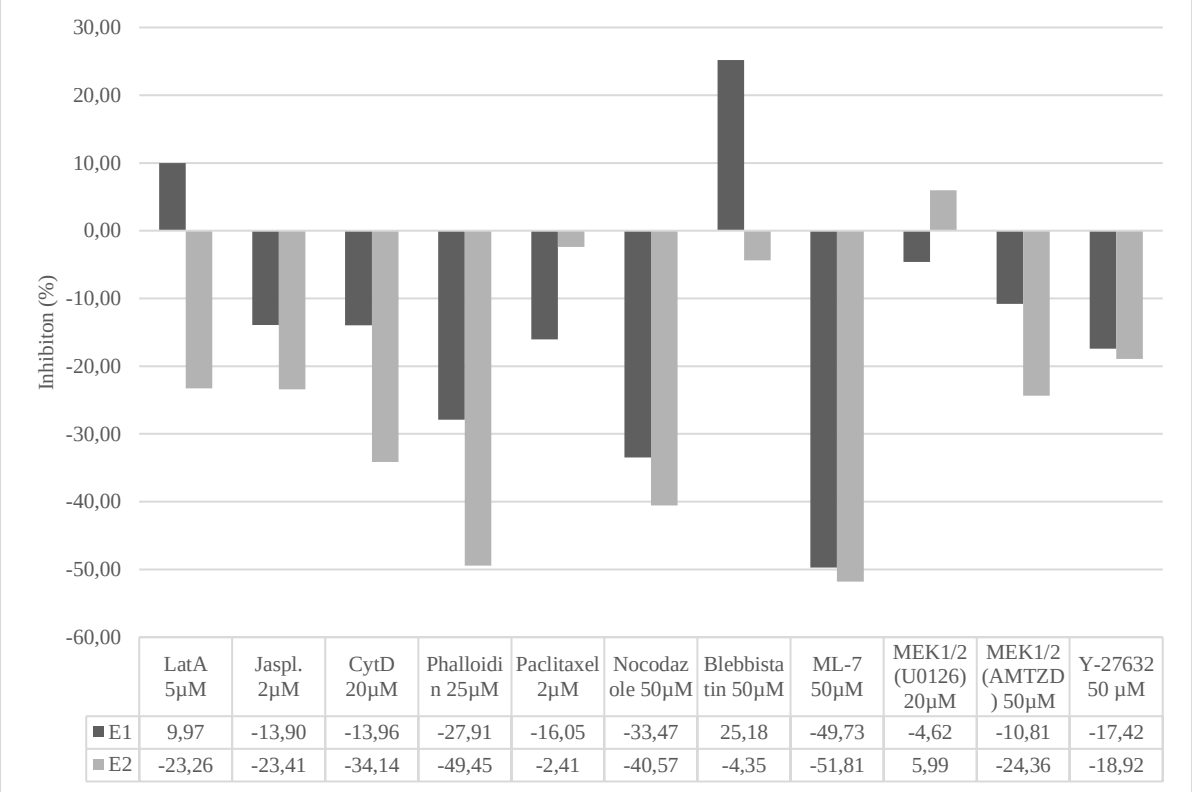

	LatA 5µM	Jaspl. 2µM	CytD 20µM	Phalloidin 25µM	Paclitaxel 2µM	Nocodazole 50µM	Blebbistatin 50µM	ML-7 50µM	MEK1/2 (U0126) 20µM	MEK1/2 (AMTZD) 50µM	Y-27632 50 µM
E1	9,97	-13,90	-13,96	-27,91	-16,05	-33,47	25,18	-49,73	-4,62	-10,81	-17,42
E2	-23,26	-23,41	-34,14	-49,45	-2,41	-40,57	-4,35	-51,81	5,99	-24,36	-18,92

Figure 1. The level of inhibition of CVB3 infection is given in percentage points (p.p.). In both experiments the number of CVB3-mAb labeled cells (%) was measured. The level of inhibition was calculated from the difference between the number of CVB3-mAb labeled cells in the inhibited and uninhibited (CVB3 only

As seen in the graph (Figure 1.), most inhibitors expressed higher inhibition in the E2 experiment where the number of CVB3-infected cells was also higher in the positive control (C). The level of inhibition was calculated for each inhibitor by comparing the number of inhibited and CVB3-Mab labeled cells (%) of the sample (S) to the positive control (C).

$$Inhibiton\ (\%) = \frac{(S - C)}{C}\ x\ 100$$

The results from two separate flow cytometry experiments is shown in Table 4.1. The inhibition is given as a percentage (%) for each inhibitor in both experiments separately (Figure 1.). The mean level of inhibition (%), standard deviation (SD), and standard error of the mean (SEM) of the experiments were calculated, and the data plotted (Figure 2).

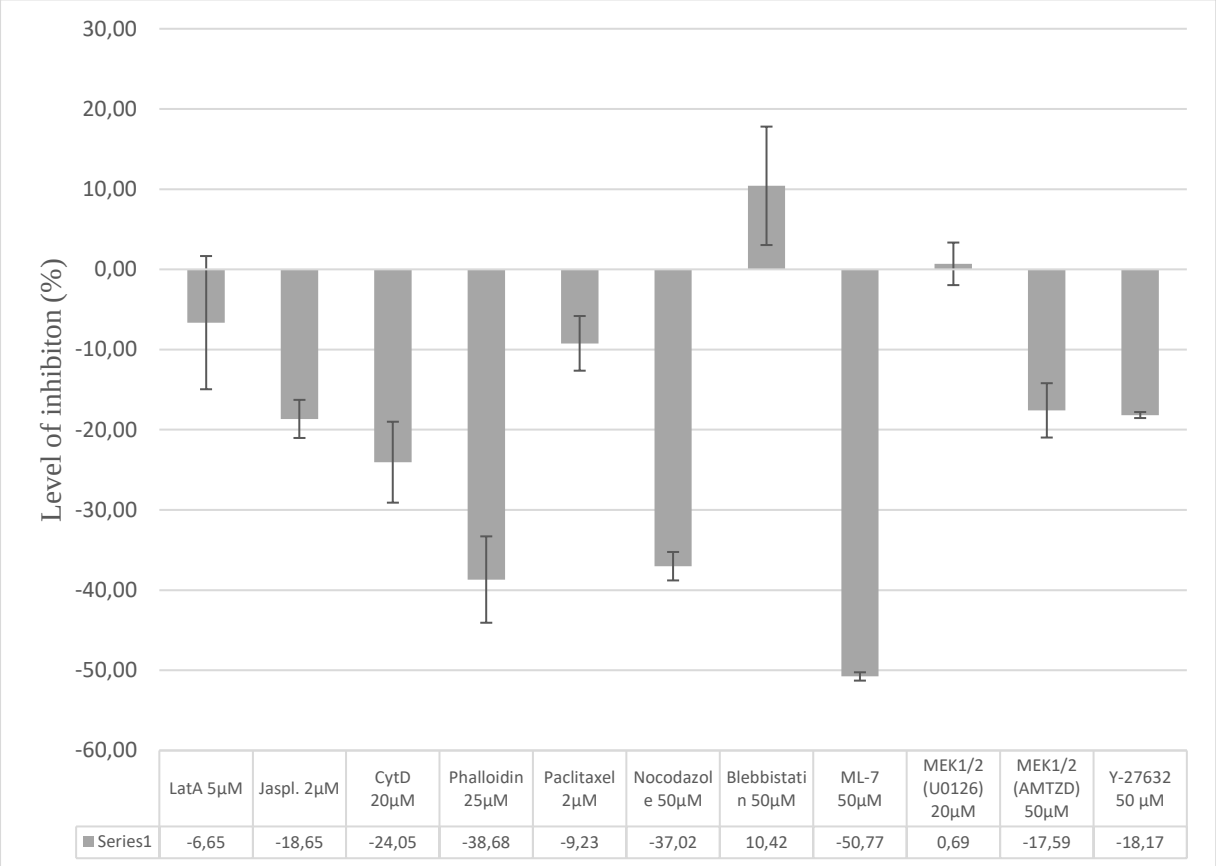

Figure 2. The level of inhibition (p.p.) of each inhibitor. The data shows the mean inhibition (p.p.) form the two separate flow cytometry experiments (E1+E2). Error bars show the standard error of the mean (SEM).

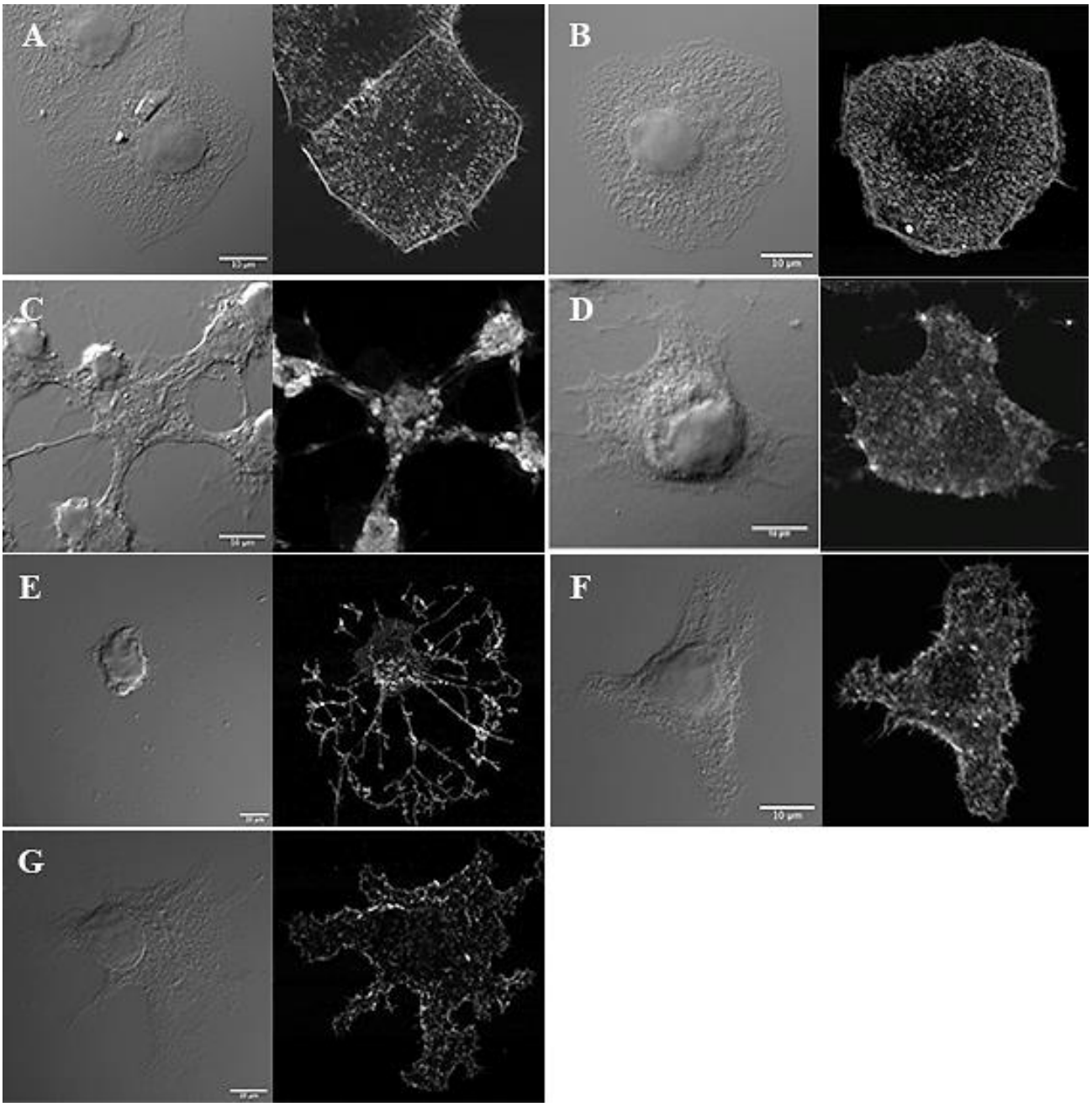

Figure 3. The effects of actin cytoskeleton inhibition in GMK cells. The actin cytoskeleton was altered by several inhibitors, either by directly interfering with actin polymerization, or via MLCK and ROCK inhibition. The control image **(A)** shows the actin cytoskeleton of a healthy GMK cell. Actin filament stabilizing drugs Phalloidin (25 µM) and Jasplakinolide (2 µM) treatments had different effects on the actin cytoskeleton. Phalloidin "freezed" the actin filaments **(B)** and the cells looked similar to the control cells **(A).** JAS treated cells had actin clusters in the cells and the morphology was drastically altered **(C).** Several JAS treated cells showed signs of cell death. Actin depolymerizing drugs CytD (20 µM) and LatA (2 µM) also had different morphological effects on the actin cytoskeleton. Most of the CytD treated cells had lost the normal cell morphology and actin cytoskeleton was partly disrupted **(D).** LatA destroyed the actin cytoskeleton of the cells almost completely and increased the number of cells that showed signs of apoptosis **(E).** Both ML-7 (50 µM) and Y-27632 (50 µM) inhibit MLC and both treatments a had similar effect on the actin filaments. Like CytD **(D)**, the

ML-7 **(F)** and Y-27632 **(G)** treated cells had an irregular shape which is due to the loss of stress fibers. The cells were cultured for 24 hours. The inhibitors were added after 12 hours and the cells were fixed with 4% PFA after 24 hours. The actin cytoskeleton was labeled with FITC-Phalloidin. Scale bars 10 µm.

4.2. Confocal images of actin cytoskeleton

Control images for actin cytoskeleton were taken from both uninfected (Fig 4A) and CVB3 infected cells (Fig 4A-C). The CVB3-induced morphological changes to the actin cytoskeleton and cellular protrusions occurred in several GMK cells. The actin filaments were visualized with FITC-Phalloidin and viral particles were first labeled with CVB3 Ab followed by anti-rabbit Alexa Fluor 555 (made in goat) secondary antibody.

4.2.1. Phalloidin – actin filament stabilizing inhibitor

Phalloidin stabilizes actin filaments and "freezes" the actin cytoskeleton. The GMK cells treated with phalloidin (25µM) did not show any abnormal morphological changes (Fig 3B). The CVB3-infected and phalloidin treated cells (Fig. 4B-C) looked similar to the uninhibited CVB3 infected cells (Fig 4A). The CVB3-induced cellular protrusions were present in the infected cells that were treated with phalloidin, however, progeny CVB3 viral capsids were not found in the adjacent cells (Fig. 4B-C).

4.2.2. Jasplakinolide – actin filament stabilizing

Jasplakinolide (JAS) is another actin stabilizing agent originally isolated from marine sponge which both inhibits F-actin depolymerization and promotes actin polymerization. Some of the JAS (2 µM) treated cells appeared apoptotic and the agent severely affected the cellular morphology of the cells (Fig. 3C). Actin was found in cluster-like structures and similar clusters were seen in the CVB3-infected, JAS inhibited cells (Fig. 4D-E). CVB3 particles were seen in filamentous structures in some JAS treated CVB3 infected cells (Fig. 4E).

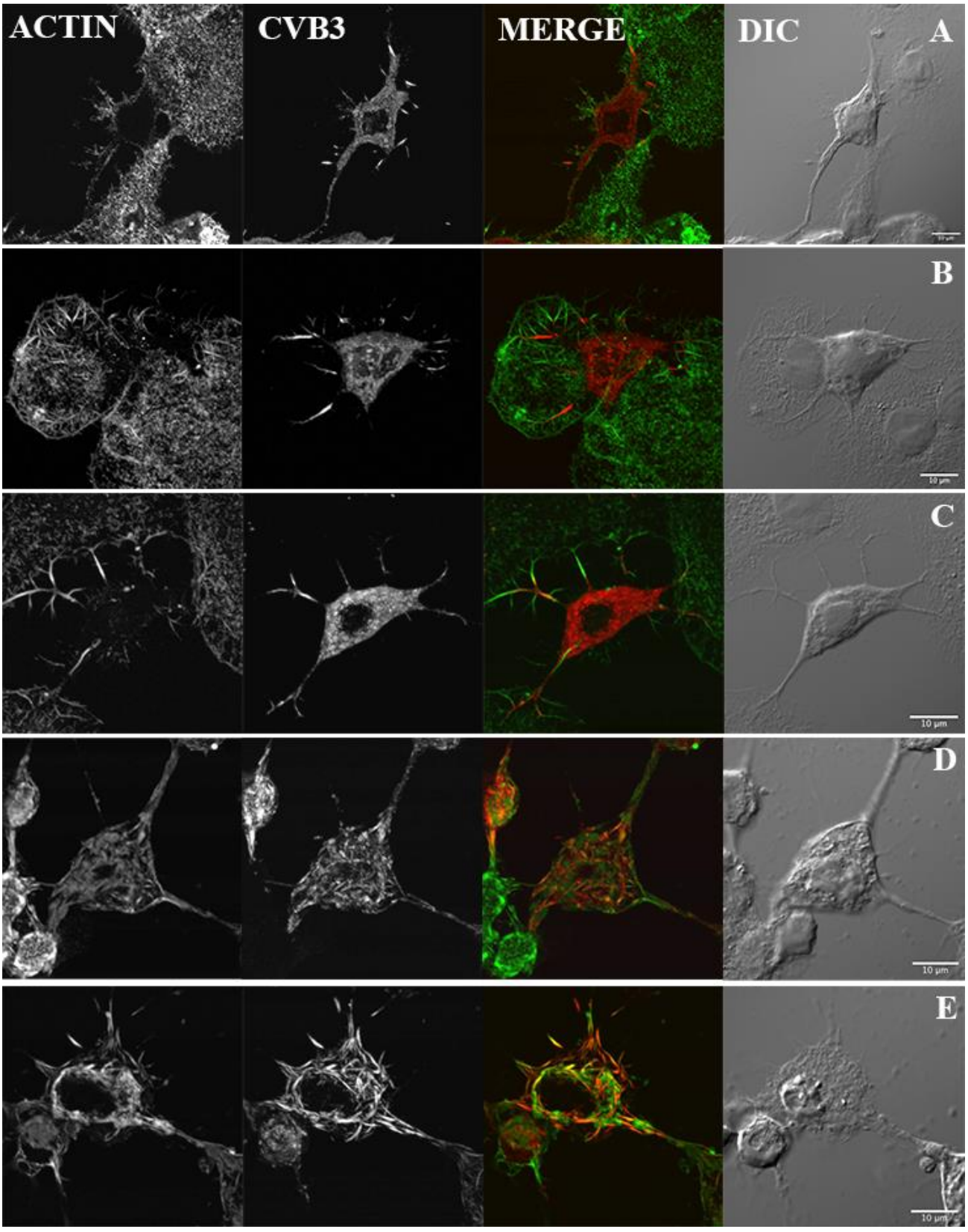
ACTIN
CVB3
MERGE
DIC
A
B
C
D
E
10 µm

Figure 4. The combined effect of actin stabilizing drugs and CVB3 infection on the GMK actin cytoskeleton. GMK cells were infected with CVB3, the agents were added 12 hpi and the cells were fixed with PFA at 24 hpi. The Phalloidin (25 µM) treated and CVB3 infected cells **(B-C)** were visually similar to CVB3-infected control cells **(A)**. The uninfected neighboring cells appeared normal and CVB3 particles (red) were seen in most of the cellular protrusions in the Phalloidin treated cells **(B-C)**. The cell's morphology had changed dramatically in the Jasplakinolide (20 µM) treated and CVB3 infected cells **(D-E)**. The actin cytoskeleton was mostly lost, and actin clusters were seen in both CVB3 infected and uninfected cells. CVB3 particles formed filamentous structures in some Jasplakinolide treated cells **(E)**. In all images the viral particles (red) were labeled with CVB3 Ab followed by anti-Rabbit AF555-conjugated secondary antibody; actin cytoskeleton (green) was visualized with FITC-Phalloidin. Scale bars 10 µm.

4.2.3 Cytochalasin D - actin depolymerizing

Cytochalasin's are a group of fungal metabolites that inhibit both actin polymerization and depolymerization. Cytochalasin D (CytD) gaps the fast-growing (barbed) end of F-actin and inhibits both the assembly and disassembly of actin. CytD (20 µM) treated GMK cells (Fig. 4D) had an irregular shape and the actin network was more dispersed than in control cells (Fig. 4A). The actin cytoskeleton was disrupted in most of the CVB3-infected and CytD inhibited cells (Fig. 5B).

4.2.4 Latrunculin A - actin depolymerizing

Latrunculin A (LatA) binds to the barbed sides of the actin monomers and rapidly depolymerizes the actin filaments. LatA is found in the red sea sponge *Latrunculia magnifica* and it is a widely used reagent to depolymerize actin filaments. The addition of LatA (5 µM) resulted in a drastic disruption of the actin cytoskeleton (Fig. 4E.). We saw an increased number of apoptotic-looking cells which had a damaged nucleus. The actin cytoskeleton was observed mostly around the nucleus and at the remains of the cell cytoskeleton (Fig. 4E, 6C-D). CVB3 infected and LatA treated GMK cells did not express the CVB3-induced cellular protrusions (Fig. 6C-D).

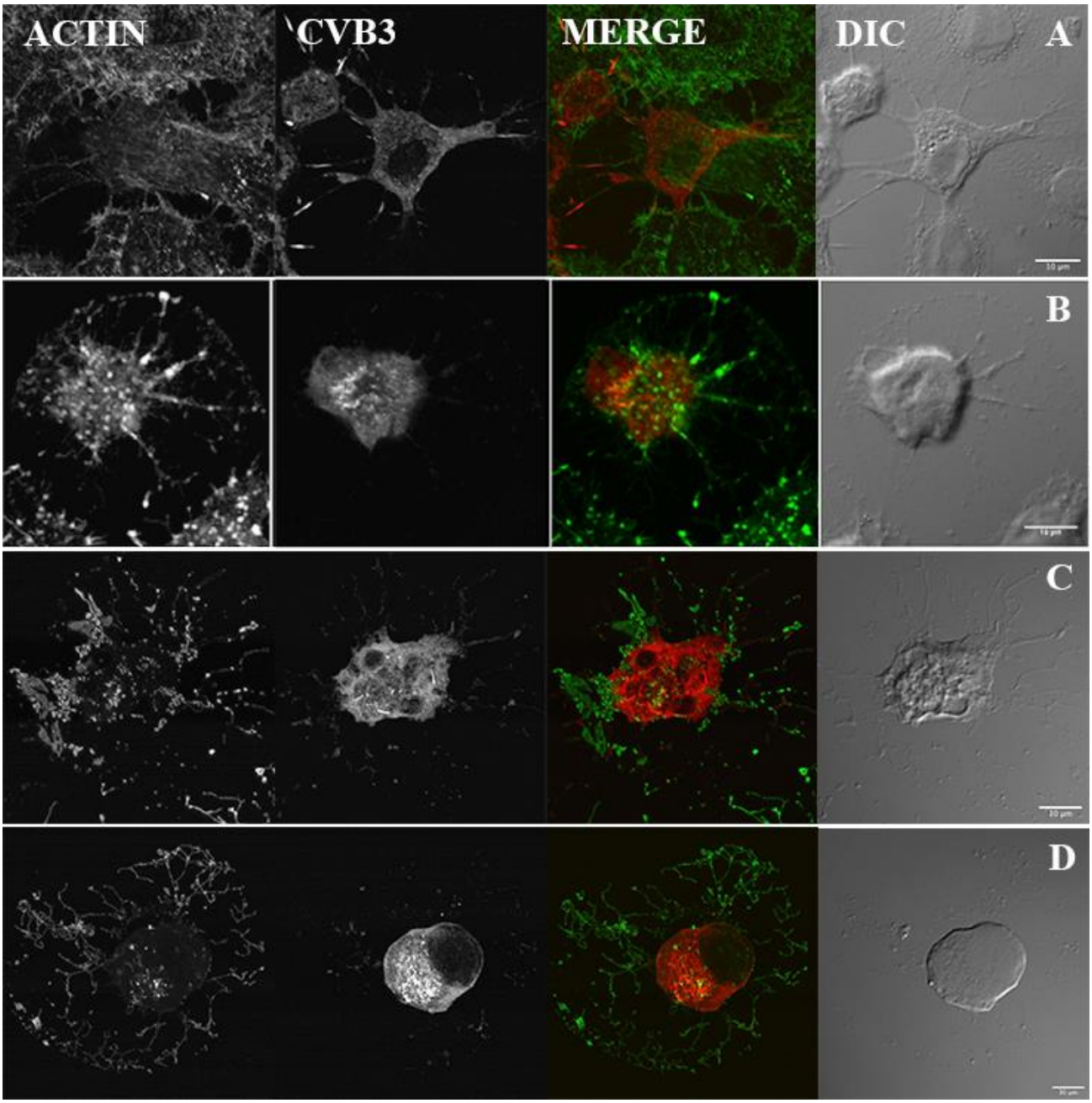

Figure 5. Actin depolymerizing drugs resulted in a drastic loss of the actin cytoskeleton. Both Cytochalasin D (20 µM) and Latrunculin A (20 µM) inhibited actin polymerization which resulted in a drastic loss of the actin cytoskeleton (green). Viral capsid protein (red) was seen in the cytosol and most of the cells did not have any CVB3-induced cellular protrusions when CVB3 infected cells were treated with CytD **(B)** or LatA **(C-D)**. Some of the CytD and LatA treated cells also showed signs of apoptosis via the loss of nucleus. The GMK cells were infected with CVB3 (MOI 0.1), and the inhibitors were added 12 hpi and the cells were fixed with 4% PFA 24 hpi. Actin (green) was labeled with FITC-Phalloidin and viral particles (red) with CVB3 Ab followed by Alexa Fluor 555 -conjugated secondary antibody. Scale bars 10 µm.

4.2.5 ML-7 – myosin light chain kinase (MLCK) inhibitor

ML-7 inhibits the phosphorylation of MLCK which has been found to prevent actin polymerization (Chen et al., 2008; Tan and Leung, 2009). Our results show that MLCK inhibition interfered with the GMK cells actin cytoskeleton morphology (Fig 3F). We also observed an increased number of small and round apoptotic cells 12 hours after adding ML-7 (50 µM) (data not shown). Some of the CVB3 infected and ML-7 treated cells (Fig 6B-C) were visually similar to the CVB3 infected control cells (Fig 6A). The virus-induced cellular protrusions were visible when treated with ML-7 (Fig 6B-C), but interestingly, viral capsid particles were not seen in the adjacent cells, unlike in most of the CVB3 infected control cells (Fig 6A).

4.2.6 Y-27632 – Rho-kinase (ROCK) inhibitor

Y-27632 (50 µM) was used to inhibit Rho kinase, an enzyme that both directly phosphorylates MLC and inhibits myosin phosphatase. The Y-27632 treated GMK cells (Fig. 3G) had an irregular shape compared to control cells (Fig. 3A) and less CVB3-induced protrusions were present when the infected cells were treated with Y-27632 (Fig. 6D). However, akin to ML-7 (Fig. 6B-C), viral capsids were not seen in the adjacent cells when treated with Y-26732 (Fig. 6D).

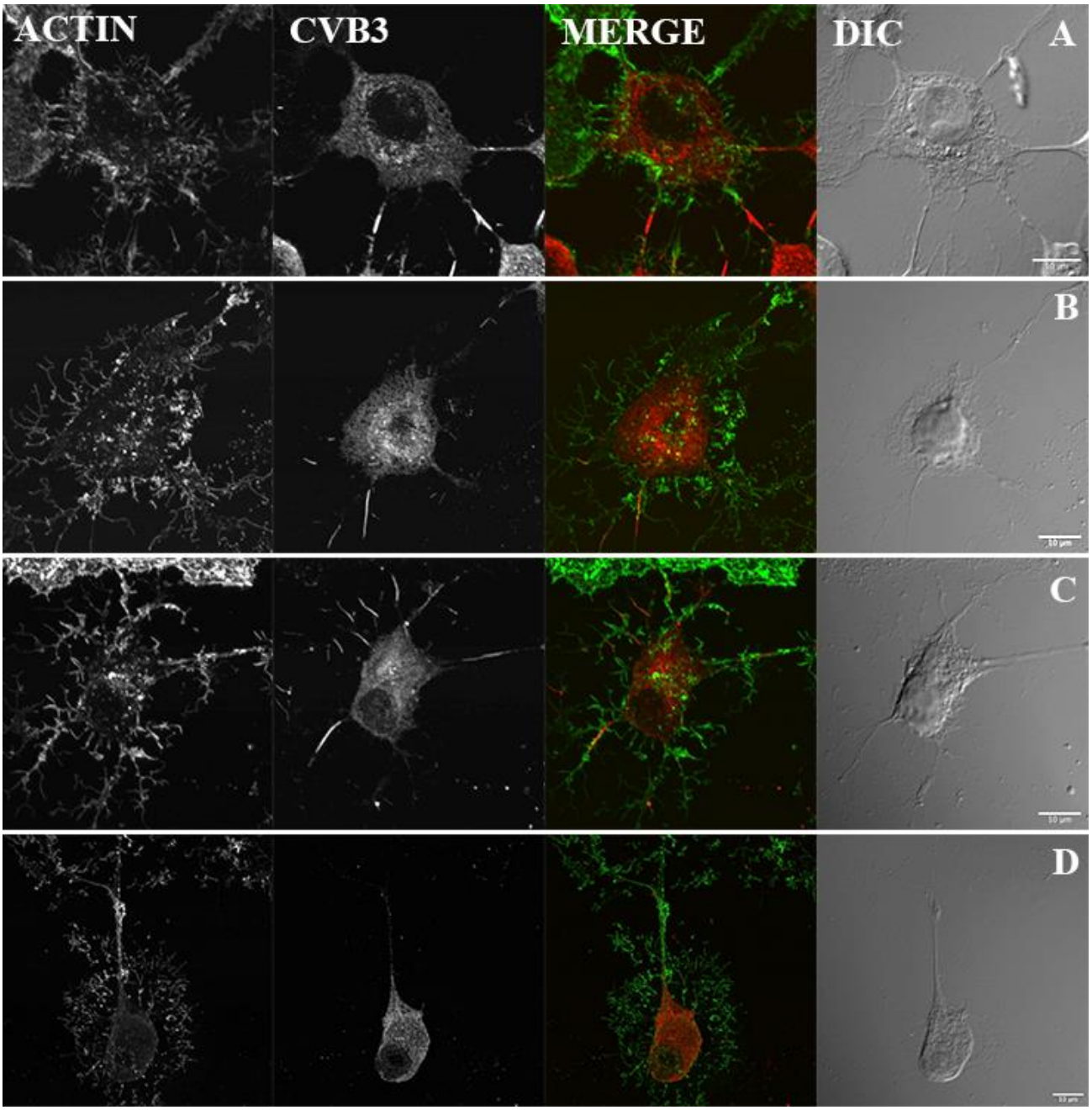

Figure 6. MLCK and ROCK inhibition in CVB3 infected cells. CVB3 infected cells were treated with ML-7 (50 µM) and Y-27632 (50 µM) 12 hpi and fixed with 4% PFA 24 hpi. Both ML-7 **(B)** and Y-27632 **(C)** inhibit MLC phosphorylation that alters the dynamics of the actin cytoskeleton (green). The ML-7 treated and CVB3 infected cells **(B)** were visually like the infected control cells **(A).** Although the CVB3-induced protrusions were observed when infected cells were treated with ML-7, the adjacent cells were not infected like in the control cells **(A)**. We saw less virus-induced cellular extensions in Y-27632 treated and CVB3 infected cells **(C).** Similarly, as with ML-7, the cells adjacent to the infected cells were found free from progeny virus particles when ROCK was inhibited with Y-27632 **(C).** The CVB3 particles (red) were labeled with CVB3 Ab and Alexa Fluor 555 -conjugated secondary Ab. Actin cytoskeleton was visualized with FITC-Phalloidin. Scale bars 10 µm.

4.3 Confocal images of microtubules

Control images show the microtubule network (MTN) of the uninfected (Figure 7A) and CVB3-infected GMK cells (Figure 8A). Infection by CVB3 did not affect microtubules but the infected cells had greater numbers of microtubule filaments at the cellular membrane (Fig 8A). Microtubules were visualized with α-tubulin mAb followed by Alexa Fluor 633-conjugated anti-Mouse secondary antibody.

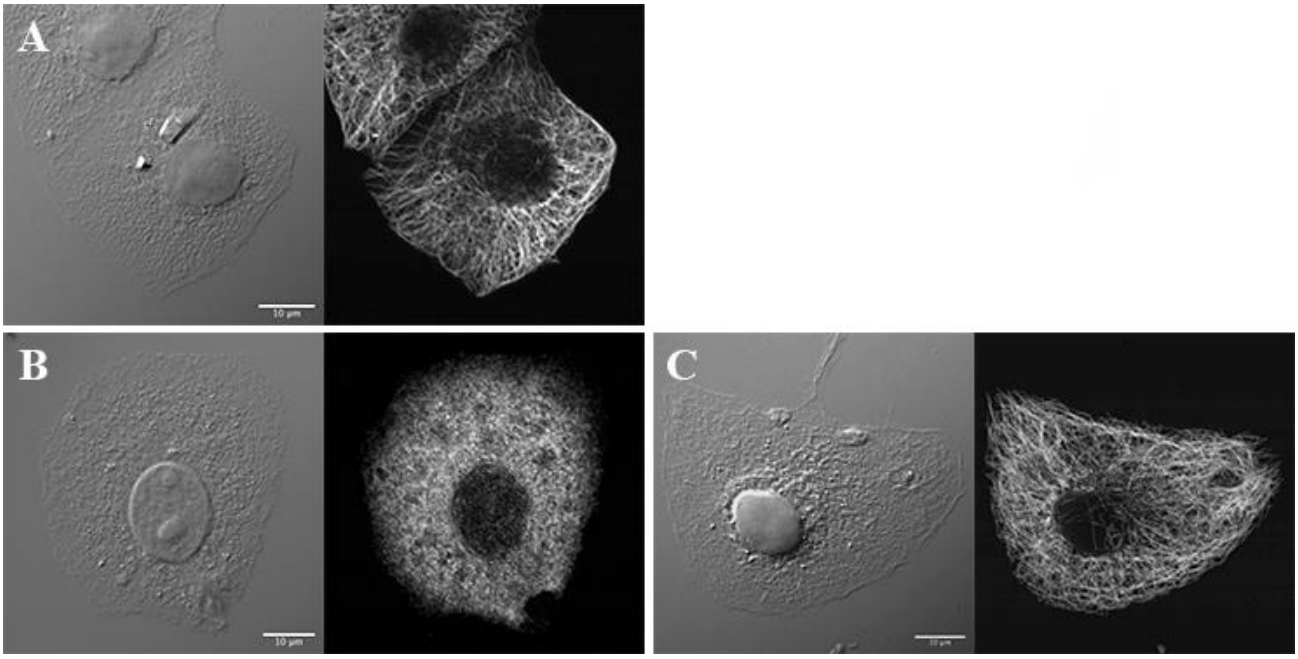

Figure 7. MTN of untreated and NOC or PAC treated GMK cells. Two MT inhibiting drugs, Nocodazole and Paclitaxel, were used to depolymerize and stabilize the MT. NOC (50 µM) prevented MT polymerization and completely disrupted the MT filaments **(B)**. However, the morphology of NOC treated cells was not altered. PAC inhibits MT depolymerization and the MTN of PAC (2 µM) treated cells **(C)** was akin to that of control cells **(A)**. Microtubules were labeled with a α-tubulin mAb followed by Alexa Fluor 633 -conjugated anti-Mouse secondary antibody. Scale bars 10 µm.

4.3.1 Nocodazole - microtubule depolymerizing

Nocodazole (NOC) inhibits microtubule assembly during mitosis and interphase. NOC binds to tubulin monomers and prevents the formation of microtubule filaments (Fig 7B, 8B) but the cellular morphology of the GMK cells was not altered (Fig 7B). Tubulin was also found in the nucleus of CVB3-infected cells treated with NOC (Figure 8B). The virus particles were highly expressed in the cellular protrusions, and inside the cytosol CVB3 particles was present in clusters (Fig 8B).

4.3.2 Paclitaxel - microtubule stabilizing

Paclitaxel (PAC) is a widely used cancer chemotherapy drug. PAC stabilizes microtubules during mitosis causing cell cycle arrest and induces apoptosis (Bacus et al., 2001). The microtubule stabilizing effect was observed in the Paclitaxel (2µM) treated GMK cells (Fig 7C, 8C). No clear difference was seen in their cell morphology when compared to the control cells (Fig 7A & 8A).

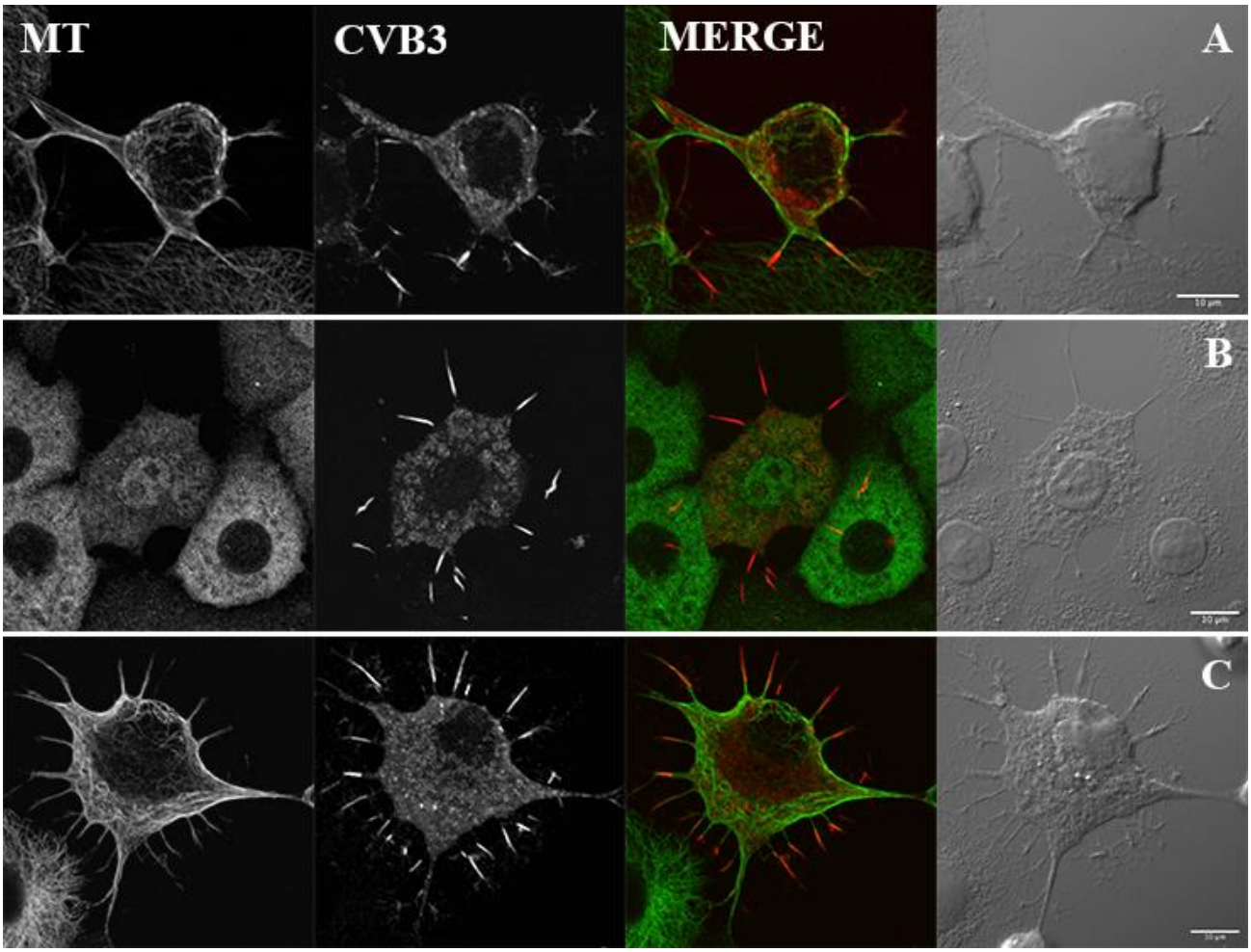

Figure 8. MTN after CVB3 infection and MT inhibition with NOC or PAC. After CVB3 infection microtubule filaments were mostly seen at the cellular membrane **(A)**. NOC (50 µM) inhibits microtubule polymerization during mitosis and completely disrupts the MT filaments. NOC prevented the CVB3-induced morphological changes and several cells revealed MTs (green) in the nucleus **(B)**. PAC (2µM) treatment stabilizes the microtubule filaments during mitosis. Several Paclitaxel treated and CVB3 infected cells **(C)** had two nuclei but otherwise the cells seemed to be like CVB3 infected control cells **(A)**. CVB3 capsid proteins (red) were seen in the virus-induced cellular protrusions when CVB3 infected cells were treated with NOC **(B)** or PAC **(C).** Microtubules (green) were visualized with α-tubulin mAb followed by anti-Mouse Alexa Fluor 633-conjugated secondary antibody, viral particles (red) were labeled with CVB3 Ab and Alexa Fluor 555 -conjugated anti-Rabbit secondary antibody. Scale bars 10 µm.

5. DISCUSSION

The actin cytoskeleton has been found to be important for nonlytic egress of several viruses (Trejo-Cerro et al., 2018; Dietzel et al., 2013; Wang et al., 2010). As showed earlier, Coxsackievirus B3 alters the morphology of GMK cell cytoskeleton and induces cellular protrusions (Paloheimo et al., 2011). These tubular blebs, rich in actin and viral capsids, were suggested as a potential novel pathway of non-lytic egress of the virus. Paloheimo et al. (2011) showed that disruption of filamentous actin with CytD prevented the formation of virus-induced cellular protrusions and that progeny CVB3 virions were found only in the cytosol. Similar effects of CytD has been previously demonstrated with measles virus (MV) (Dietzel et al., 2013). Our observations corresponded to the previous findings, that CytD prevents the formation of CVB3-induced protrusions and that virus particles were only in the cytosol due to the loss of filamentous actin cytoskeleton. Our results further indicated that filamentous actin is needed for the formation of CVB3-induced cellular protrusions.

Previously, it has been demonstrated that actin stabilization with JAS decreased the titer of MV, but interestingly, actin disruption with CytD increased the cell-to-cell spread of the virus (Dietzel et al., 2013). Dietzel et al. (2013) suggested that actin stabilization with JAS interferes with MV assembly and budding, where the dynamic cortical actin filaments are essential. In a later study, Trejo-Cerro et al. (2018) demonstrated that JAS inhibited the nonlytic egress of rotavirus progeny virion (Trejo-Cerro et al., 2018). Indeed, using confocal microscopy, we saw that JAS severely altered the cell morphology and actin network in both healthy and CVB3 infected GMK cells. Our FACS results showed that blocking filamentous actin depolymerization with JAS showed only mild inhibition in FACS, while phalloidin significantly inhibited the CVB3 infection. On the other hand, actin stabilization with JAS or Phalloidin did not prevent the formation of virus-induced protrusions in GMK cells. Confocal microscopy imaging also revealed that adjacent cells to the virus-induced cellular protrusions were found free of progeny virions when treated with phalloidin. Combined, these observations suggest that phalloidin could prevent progeny CVB3 virions spreading to adjacent cells through cellular protrusions. It has been reported that CVB3 capsid proteins are colocalized with clathrin in Hela cells (Chung et al., 2005). Chung et al. (2005) also showed that CVB3 capsid were not seen to colocalize with caveolin, thus suggesting virus entry via clathrin-mediated endocytosis.

Furthermore, Yarar et al. (2005) demonstrated that clathrin-mediated endocytosis was decreased in mammalian cells if the actin cytoskeleton was inhibited with JAS or LatA (Yarar et al., 2005). Thus, the observed inhibiting effect of actin polymerizing and depolymerizing agents to the CVB3 infection could also be due to disturbed endocytosis. Unfortunately, our results were not indicative of whether these agents inhibit the entry or exit of the virus, therefore, further studies would be needed to determine their function.

CVB3-induced protrusions were not seen when actin polymerizing was inhibited with LatA, though LatA also severely altered actin cytoskeleton morphology on both healthy and CVB3-infected cells. Inhibition of dynamic actin cytoskeleton is a known regulator of programmed cell death. Previous studies demonstrate that the disruption of actin cytoskeleton with LatA or CytD induces apoptosis (Ailenberg and Silverman, 2003; Martin and Leder, 2001). Interestingly, CytD is also found to promote cell survival due to increased phosphorylation of MEK1/2, ERK1/2 and BAD in NIH 3T3 cells. (Ailenberg and Silverman, 2003). CytD has also been found to increase caspase-3-mediated cytochrome c release in HeLa cells, indicating that F-actin damage with CytD activated an apoptotic signaling pathway. Paul et al. (2002) also demonstrated that pretreatment of HeLa cells with the actin stabilizing agent, phalloidin, managed to delay cytochrome c release (Paul et al., 2002). JAS has also been shown to increase apoptosis in several cell lines (Rao et al., 1999; Odaka et al., 2000). Odaka et al. (2000) suggested that JAS induced apoptosis is caused by a caspase-3-like protease-dependent pathway (Odaka et al., 2000). Indeed, using confocal microscopy, we saw an increased number of cells with signs of cell death when GMK cells were treated with LatA, CytD and JAS. Further, the images showed drastic changes in cell morphology and the actin cytoskeleton. Previous studies have also shown that inhibition of MLCK with ML-7 leads to the dephosphorylation of nonmuscle myosin II and induces apoptosis (Fazal et al., 2005; Connell and Helfman, 2006). ML-7 selectively inhibits myosin light chain kinase and prevents the phosphorylation of the 20 kDa light chain of nonmuscle myosin II (MLC_{20}). Although ML-7 showed the strongest inhibition to the CVB3 infection in our FACS experiments, MLCK inhibition also increased the number of several small and round, apoptotic-looking cells, as seen in the confocal imaging. However, in the absence of apoptotic markers available for confocal imaging, the inhibitor-induced apoptotic changes of the host cells remained

undetectable. Future studies should be performed where the apoptotic markers in FACS and chromatin are accurately visualized using confocal microscopy imaging as a means to confirm our observations.

ROCK, a myosin light chain activating protein, is known to both inhibit myosin phosphatase activity, which results in increased phosphorylation of MLC, and directly phosphorylate MLC (Totsukawa et al., 2000). ROCK also induces stress fiber and focal adhesion formation in fibroblasts (Katoh, 2017) and the inhibition of ROCK has been found to affect the actomyosin contractility in both muscle and nonmuscle cells (Totsukawa et al., 2000). Similarly, we saw the loss of stress fibers and focal adhesion in uninfected GMK cells when ROCK or MLCK was inhibited. As previously described, several ML-7 treated cells appeared to be apoptotic. Interestingly, nonapoptotic looking ML-7 treated cells and all the Y-27632 treated GMK cells, had lost their normal morphology, likely due to the loss of focal adhesions. Inhibition of MLCK-mediated phosphorylation of MLC has been found effective towards HSV-1 and HIV-1 infection (Haidari et al., 2011; Antoine and Shukla, 2014; Sasaki et al., 1995). Similarly, the inhibition of ROCK1 has been found to interfere both the release and cell-to-cell transmission of HIV-1 (Wen et al., 2014). According to our FACS results, inhibition of ROCK with Y-27632, showed only mild inhibition. In confocal microscopy, we were able to observe CVB3 particle containing cellular membrane extensions when CVB3-infected cells were treated with Y-27632. However, we saw fewer infected cells with virus-induced cellular protrusions when treated with Y-27632 and CVB3 particles were mostly seen in the cytosol. Our observations suggest that inhibition of ROCK with Y-27632 could be important for the formation of CVB3-induced protrusions. As our studies showed, MLCK inhibition with ML-7 did not prevent the formation of CVB3-induced protrusions. Also, since ROCK is known to have diverse functions in the cell (Julian and Olson, 2014), the initial effects of ROCK inhibition on the formation of virus-induced extensions could be the result of something other than MLC inhibition. We recommend that further studies should be performed to investigate the mechanisms of ROCK inhibition on the CVB3 induced cellular protrusions.

Several viruses exploit the MTs of host cells during their entry and egress (Simpson and Yamauchi, 2020). For example, MT disruption with NOC has been shown to inhibit the release of progeny Rice gall dwarf virus out of the host cell (Wei et al., 2006). Similarly, Simon et al. (2008) found that MT depolymerization with NOC significantly decreased the titer of progeny Crimean-Congo hemorrhagic

fever virus (CCHFV) whereas MT stabilization with PAC only slightly affected the virus titer. However, both NOC and PAC interfered with CCHFV egress (Simon et al., 2008). Certainly, our experiments showed similar results; MT depolymerization with NOC inhibited the CVB3 infection but MT filament stabilization with PAC showed only some inhibition of the viral infection. Previous studies have shown that clathrin-mediated endocytosis is inhibited during Nocodazole-mediated mitotic arrest (Tacheva-Grigorova et al., 2013; Fielding et al., 2012). Furthermore, it has been demonstrated that NOC inhibited the infection of the DAF-binding strain of echovirus 11 (EV11-207) but did not inhibit the infection of a non-DAF-binding strain, EV-207R. In their study, Stuart et al. (2002) suggested that constant inhibition with NOC could prevent several trafficking pathways from clathrin-coated pits, lipid rafts and caveolae (Stuart et al., 2002). Thus, the inhibition of NOC observed in our FACS results, could be due to the impaired receptor-mediated endocytosis that CVB3 uses in the entry to the host cell.

Previously, Paloheimo et al. (2011) reported that depolymerization of microtubule filaments with NOC did not prevent the emergence of CVB3-induced protrusions (Paloheimo et al., 2011). Our results concur with these initial findings; CVB3-induced protrusions were observed when GMK cells were infected with CVB3 and treated with NOC or PAC. Our findings further demonstrate that MTN does not have an essential role in protrusion formation. Microtubule depolymerization has been reported to induce stress fiber and focal adhesion formations on 3T3 cells through the activation of Rho (Liu et al., 1998). In this study we did not observe the effects of these microtubule inhibitors on the actin cytoskeleton. However, the suggested Rho-induced activation of stress fiber and focal adhesion formation could explain why GMK cell morphology was not affected when CVB3-infected cells were treated with NOC.

Conclusions

We have demonstrated that the inhibition of the actin cytoskeleton, of ROCK, of MLCK and of the MTs effectively inhibits CVB3 infection. Fewer numbers of CVB3 infected GMK cells were observed in FACS when the cells were simultaneously infected with CVB3 and treated with different inhibitors affecting the dynamic actin cytoskeleton, microtubules, ROCK or MLCK. Our results showed that

MT depolymerization with NOC significantly inhibited the CVB3 infection. However, we also demonstrated that microtubules are not essential for the appearance of the CVB3-induced protrusions. Thus, the inhibition of NOC on CVB3 infection is likely due to the disturbed receptor-mediated entry into the host cell. We highlighted that, actin cytoskeleton disruption with CytD or LatA prevents the formation of virus-induced protrusions, further demonstrating that actin is essential for the formation of CVB3-induced cellular extensions. An actin filament stabilizing agent, phalloidin, did not prevent the emergence of virus-induced extensions, but, interestingly, the progeny CVB3 particles were not found in the adjacent cells. Our findings suggest that, phalloidin effectively interferes either with the entry or egress of progeny CVB3 particles. However, further studies should be performed to confirm the initial effects of phalloidin-mediated inhibition on CVB3 infection. Although both MLCK and ROCK are known to phosphorylate MLC, our results suggest that the mechanisms of MLCK and ROCK inhibition on CVB3 infection differ. Here, we showed that inhibition of ROCK with Y-27632 was able to hinder the formation of CVB3-induced protrusions, and the CVB3 particles were seen mostly in the cytosol, while MLCK inhibition with ML-7 did not prevent the emergence of virus-induced protrusions. Further studies should be carried out to distinguish the mechanism of ROCK inhibition on CVB3 infection and virus-induced cellular protrusions.

Acknowledgments

Firstly, I want to thank my supervisor docent Maija Vihinen-Ranta for the opportunity to do my thesis work in the research group and for the endless support and guidance to complete my thesis writing. I want to thank Outi Paloheimo (MSc) whose preliminary work with CVB3 provided the starting point of my thesis. Thank you Outi for your help, supervision, and inspiration. Additionally, I would like to thank all the former lab members and friends (Elina, Visa, Jori, Sami, Vesa, Jarkko and Alli) for the fun times when I was doing the lab work for this thesis. Finally, I want to thank my family and friends supporting and believing in me to finish my thesis.

REFERENCES

Ailenberg, M. and M. Silverman. 2003. Cytochalasin D disruption of actin filaments in 3T3 cells produces an anti-apoptotic response by activating gelatinase A extracellularly and initiating intracellular survival signals. *Biochimica Et Biophysica Acta (BBA) - Molecular Cell Research.* 1593:249-258. doi: 10.1016/S0167-4889(02)00395-6.

Amano, M., M. Nakayama and K. Kaibuchi. 2010. Rho-kinase/ROCK: A key regulator of the cytoskeleton and cell polarity. *Cytoskeleton (Hoboken, N.J.).* 67:545-554. doi: 10.1002/cm.20472.

Antoine, T.E. and D. Shukla. 2014. Inhibition of myosin light chain kinase can be targeted for the development of new therapies against herpes simplex virus type-1 infection. *Antivir. Ther. (Lond.).* 19:15-29. doi: 10.3851/IMP2661.

Bacus, S.S., A.V. Gudkov, M. Lowe, L. Lyass, Y. Yung, A.P. Komarov, K. Keyomarsi, Y. Yarden and R. Seger. 2001. Taxol-induced apoptosis depends on MAP kinase pathways (ERK and p38) and is independent of p53. *Oncogene.* 20:147-155. doi: 10.1038/sj.onc.1204062.

Bearer, E.L. and P. Satpute-Krishnan. 2002. The Role of the Cytoskeleton in the Life Cycle of Viruses and Intracellular Bacteria: Tracks, Motors, and Polymerization Machines. *Curr Drug Targets Infect Disord.* 2:247-264.

Bird, S.W. and K. Kirkegaard. 2015. Nonlytic spread of naked viruses. *Autophagy.* 11:430-431. doi: 10.4161/15548627.2014.994372.

Bukrinskaya, A., B. Brichacek, A. Mann and M. Stevenson. 1998. Establishment of a functional human immunodeficiency virus type 1 (HIV-1) reverse transcription complex involves the cytoskeleton. *The Journal of Experimental Medicine.* 188:2113-2125.

Chen, X., K. Pavlish and J.N. Benoit. 2008. Myosin phosphorylation triggers actin polymerization in vascular smooth muscle. *Am J Physiol Heart Circ Physiol.* 295:H2172-H2177. doi: 10.1152/ajpheart.91437.2007.

Chung, S., J. Kim, I. Kim, S. Park, K. Paek and J. Nam. 2005. Internalization and trafficking mechanisms of coxsackievirus B3 in HeLa cells. *Virology.* 333:31-40. doi: 10.1016/j.virol.2004.12.010.

Connell, L.E. and D.M. Helfman. 2006. Myosin light chain kinase plays a role in the regulation of epithelial cell survival. *J. Cell. Sci.* 119:2269-2281. doi: 10.1242/jcs.02926.

Coyne, C.B. and J.M. Bergelson. 2006. Virus-Induced Abl and Fyn Kinase Signals Permit Coxsackievirus Entry through Epithelial Tight Junctions. *Cell (Cambridge).* 124:119-131. doi: 10.1016/j.cell.2005.10.035.

Cudmore, S., P. Cossart, G. Griffiths and M. Way. 1995. Actin-based motility of vaccinia virus. *Nature.* 378:636-638. doi: 10.1038/378636a0.

Dietzel, E., L. Kolesnikova and A. Maisner. 2013. Actin filaments disruption and stabilization affect measles virus maturation by different mechanisms. *Virol. J.* 10:249. doi: 10.1186/1743-422X-10-249.

Fazal, F., L. Gu, I. Ihnatovych, Y. Han, W. Hu, N. Antic, F. Carreira, J.F. Blomquist, T.J. Hope, D.S. Ucker and P. de Lanerolle. 2005. Inhibiting myosin light chain kinase induces apoptosis in vitro and in vivo. *Molecular and Cellular Biology.* 25:6259-6266.

Feng, Z., L. Hensley, K.L. McKnight, F. Hu, V. Madden, L. Ping, S. Jeong, C. Walker, R.E. Lanford and S.M. Lemon. 2013. A pathogenic picornavirus acquires an envelope by hijacking cellular membranes. *Nature.* 496:367-371. doi: 10.1038/nature12029.

Fielding, A.B., A.K. Willox, E. Okeke and S.J. Royle. 2012. Clathrin-mediated endocytosis is inhibited during mitosis. *Proc Natl Acad Sci U S A.* 109:6572-6577. doi: 10.1073/pnas.1117401109.

Gil, P.I., G. Albrieu-Llinás, E.C. Mlewski, M. Monetti, L. Fozzatti, C. Cuffini, J.F. Romero, P. Kunda and M.G. Paglini. 2017. Pixuna virus modifies host cell cytoskeleton to secure infection. *Scientific Reports.* 7:1-9. doi: 10.1038/s41598-017-05983-w.

Haidari, M., W. Zhang, L. Ganjehei, M. Ali and Z. Chen. 2011. Inhibition of MLC Phosphorylation Restricts Replication of Influenza Virus—A Mechanism of Action for Anti-Influenza Agents. *PLoS One.* 6. doi: 10.1371/journal.pone.0021444.

Hashimoto, M., F. Bhuyan, M. Hiyoshi, O. Noyori, H. Nasser, M. Miyazaki, T. Saito, Y. Kondoh, H. Osada, S. Kimura, K. Hase, H. Ohno and S. Suzu. 2016. Potential Role of the Formation of Tunneling Nanotubes in HIV-1 Spread in Macrophages. *J. Immunol.* 196:1832-1841. doi: 10.4049/jimmunol.1500845.

Iyengar, S., J.E.K. Hildreth and D.H. Schwartz. 1998. Actin-Dependent Receptor Colocalization Required for Human Immunodeficiency Virus Entry into Host Cells. *J Virol.* 72:5251-5255.

Julian, L. and M.F. Olson. 2014. Rho-associated coiled-coil containing kinases (ROCK). *Small GTPases.* 5. doi: 10.4161/sgtp.29846.

Katoh, K. 2017. Activation of Rho-kinase and focal adhesion kinase regulates the organization of stress fibers and focal adhesions in the central part of fibroblasts. *PeerJ.* 5. doi: 10.7717/peerj.4063.

Lehmann, M.J., N.M. Sherer, C.B. Marks, M. Pypaert and W. Mothes. 2005. Actin- and myosin-driven movement of viruses along filopodia precedes their entry into cells. *J. Cell Biol.* 170:317-325. doi: 10.1083/jcb.200503059.

Liu, B.P., M. Chrzanowska-Wodnicka and K. Burridge. 1998. Microtubule Depolymerization Induces Stress Fibers, Focal Adhesions, and DNA Synthesis via the GTP-Binding Protein Rho. *Cell Adhesion and Communication.* 5:249-255. doi: 10.3109/15419069809040295.

Lyman, M.G. and L.W. Enquist. 2009. Herpesvirus Interactions with the Host Cytoskeleton. *J Virol.* 83:2058-2066. doi: 10.1128/JVI.01718-08.

Martin, S.S. and P. Leder. 2001. Human MCF10A mammary epithelial cells undergo apoptosis following actin depolymerization that is independent of attachment and rescued by Bcl-2. *Mol Cell Biol.* 21:6529-6536. doi: 10.1128/mcb.21.19.6529-6536.2001.

Milstone, A.M., J. Petrella, M.D. Sanchez, M. Mahmud, J.C. Whitbeck and J.M. Bergelson. 2005. Interaction with Coxsackievirus and Adenovirus Receptor, but Not with Decay-Accelerating Factor (DAF), Induces A-Particle Formation in a DAF-Binding Coxsackievirus B3 Isolate. *J Virol.* 79:655-660. doi: 10.1128/JVI.79.1.655-660.2005.

Munjal, A. and T. Lecuit. 2014. Actomyosin networks and tissue morphogenesis. *Development.* 141:1789-1793. doi: 10.1242/dev.091645.

Odaka, C., M.L. Sanders and P. Crews. 2000. Jasplakinolide induces apoptosis in various transformed cell lines by a caspase-3-like protease-dependent pathway. *Clin Diagn Lab Immunol.* 7:947-952. doi: 10.1128/cdli.7.6.947-952.2000.

Paloheimo, O., T.O. Ihalainen, S. Tauriainen, O. Välilehto, S. Kirjavainen, E.A. Niskanen, J.P. Laakkonen, H. Hyöty and M. Vihinen-Ranta. 2011. Coxsackievirus B3-Induced Cellular Protrusions: Structural Characteristics and Functional Competence ▿ . *J Virol.* 85:6714-6724. doi: 10.1128/JVI.00247-10.

Paul, C., F. Manero, S. Gonin, C. Kretz-Remy, S. Virot and A. Arrigo. 2002. Hsp27 as a Negative Regulator of Cytochrome c Release. *Mol Cell Biol.* 22:816-834. doi: 10.1128/MCB.22.3.816-834.2002.

Rao, J.Y., Y.S. Jin, Q. Zheng, J. Cheng, J. Tai and G.P. Hemstreet. 1999. Alterations of the actin polymerization status as an apoptotic morphological effector in HL-60 cells. *J Cell Biochem.* 75:686-697.

Rustom, A., R. Saffrich, I. Markovic, P. Walther and H. Gerdes. 2004. Nanotubular highways for intercellular organelle transport. *Science.* 303:1007-1010. doi: 10.1126/science.1093133.

Sasaki, H., M. Nakamura, T. Ohno, Y. Matsuda, Y. Yuda and Y. Nonomura. 1995. Myosin-actin interaction plays an important role in human immunodeficiency virus type 1 release from host cells. *Proc Natl Acad Sci U S A.* 92:2026-2030.

Schelhaas, M., H. Ewers, M. Rajamäki, P.M. Day, J.T. Schiller and A. Helenius. 2008. Human Papillomavirus Type 16 Entry: Retrograde Cell Surface Transport along Actin-Rich Protrusions. *PLoS Pathog.* 4. doi: 10.1371/journal.ppat.1000148.

Simon, M., C. Johansson, Å Lundkvist and A. Mirazimi. 2008. Microtubule-dependent and microtubule-independent steps in Crimean-Congo hemorrhagic fever virus replication cycle. *Virology.* 385:313-322. doi: 10.1016/j.virol.2008.11.020.

Simpson, C. and Y. Yamauchi. 2020. Microtubules in Influenza Virus Entry and Egress. *Viruses.* 12. doi: 10.3390/v12010117.

Smith, J.L., D.S. Lidke and M.A. Ozbun. 2008. Virus activated filopodia promote human papillomavirus type 31 uptake from the extracellular matrix. *Virology.* 381:16-21. doi: 10.1016/j.virol.2008.08.040.

Stanway, G. and T. Hyypiä. 1999. Parechoviruses. *J Virol.* 73:5249-5254.

Stuart, A.D., H.E. Eustace, T.A. McKee and T.D.K. Brown. 2002. A Novel Cell Entry Pathway for a DAF-Using Human Enterovirus Is Dependent on Lipid Rafts. *J Virol.* 76:9307-9322. doi: 10.1128/JVI.76.18.9307-9322.2002.

Tacheva-Grigorova, S.K., A.J.M. Santos, E. Boucrot and T. Kirchhausen. 2013. Clathrin-Mediated Endocytosis Persists during Unperturbed Mitosis. *Cell Rep.* 4. doi: 10.1016/j.celrep.2013.07.017.

Tan, I. and T. Leung. 2009. Myosin light chain kinases. *Cell Adh Migr.* 3:256-258.

Totsukawa, G., Y. Yamakita, S. Yamashiro, D.J. Hartshorne, Y. Sasaki and F. Matsumura. 2000. Distinct roles of ROCK (Rho-kinase) and MLCK in spatial regulation of MLC phosphorylation for assembly of stress fibers and focal adhesions in 3T3 fibroblasts. *J. Cell Biol.* 150:797-806. doi: 10.1083/jcb.150.4.797.

Tracy, S., K. Höfling, S. Pirruccello, P.H. Lane, S.M. Reyna and C.J. Gauntt. 2000. Group B coxsackievirus myocarditis and pancreatitis: connection between viral virulence phenotypes in mice. *J. Med. Virol.* 62:70-81. doi: 10.1002/1096-9071(200009)62:13.0.co;2-r.

Trejo-Cerro, Ó, C. Eichwald, E.M. Schraner, D. Silva-Ayala, S. López and C.F. Arias. 2018. Actin-Dependent Nonlytic Rotavirus Exit and Infectious Virus Morphogenetic Pathway in Nonpolarized Cells. *J.Virol.* 92:2076. doi: 10.1128/JVI.02076-17.

Vorster, P.J., J. Guo, A. Yoder, W. Wang, Y. Zheng, X. Xu, D. Yu, M. Spear and Y. Wu. 2011. LIM Kinase 1 Modulates Cortical Actin and CXCR4 Cycling and Is Activated by HIV-1 to Initiate Viral Infection. *The Journal of Biological Chemistry.* 286:12554-12564. doi: 10.1074/jbc.M110.182238.

Walsh, D. and M.H. Naghavi. 2019. Exploitation of cytoskeletal networks during early viral infection. *Trends Microbiol.* 27:39-50. doi: 10.1016/j.tim.2018.06.008.

Wang, J., J. Zhang, W. Chen, X. Xu, N. Gao, D. Fan and J. An. 2010. Roles of small GTPase Rac1 in the regulation of actin cytoskeleton during dengue virus infection. *PLoS Negl Trop Dis.* 4. doi: 10.1371/journal.pntd.0000809.

Wei, T., A. Kikuchi, Y. Moriyasu, N. Suzuki, T. Shimizu, K. Hagiwara, H. Chen, M. Takahashi, T. Ichiki-Uehara and T. Omura. 2006. The Spread of Rice Dwarf Virus among Cells of Its Insect Vector Exploits Virus-Induced Tubular Structures. *J Virol.* 80:8593-8602. doi: 10.1128/JVI.00537-06.

Wen, X., L. Ding, J. Wang, M. Qi, J. Hammonds, H. Chu, X. Chen, E. Hunter and P. Spearman. 2014. ROCK1 and LIM Kinase Modulate Retrovirus Particle Release and Cell-Cell Transmission Events. *Journal of Virology.* 88:6906-6921. doi: 10.1128/JVI.00023-14.

Wong, J., J. Zhang, X. Si, G. Gao, I. Mao, B.M. McManus and H. Luo. 2008. Autophagosome supports coxsackievirus B3 replication in host cells. *J. Virol.* 82:9143-9153. doi: 10.1128/JVI.00641-08.

Yarar, D., C.M. Waterman-Storer and S.L. Schmid. 2005. A dynamic actin cytoskeleton functions at multiple stages of clathrin-mediated endocytosis. *Mol. Biol. Cell.* 16:964-975. doi: 10.1091/mbc.e04-09-0774.